RESEARCH ARTICLE | NOVEMBER 18 2020

Vortex formation in starting buoyant jets at moderate Richardson numbers

Hui-Fen Guo (郭会芬) ; Lei Gao (高磊) ; Simon C. M. Yu (余澄文)

Physics of Fluids 32, 117107 (2020)
https://doi.org/10.1063/5.0026209

Physics of Fluids ARTICLE scitation.org/journal/phf

Vortex formation in starting buoyant jets at moderate Richardson numbers

Cite as: Phys. Fluids 32, 117107 (2020); doi: 10.1063/5.0026209
Submitted: 21 August 2020 • Accepted: 28 October 2020 •
Published Online: 18 November 2020

Hui-Fen Guo (郭会芬),[1] Lei Gao (高磊),[2,a)] and Simon C. M. Yu (余澄文)[1]

AFFILIATIONS

[1]Interdisciplinary Division of Aeronautical and Aviation Engineering, The Hong Kong Polytechnic University, Kowloon, Hong Kong, China

[2]School of Aeronautics and Astronautics, Sichuan University, Chengdu 610065, China

[a)]Author to whom correspondence should be addressed: lei.gao@scu.edu.cn

ABSTRACT

In this paper, the formation process of the leading vortex ring in positively and negatively buoyant starting jets with moderate Richardson number in the range of $0.06 < |Ri| \le 0.321$ has been investigated numerically and theoretically. Using the similarity variables $|Ri|$ and $|Ri|^{2/5}$ for the positively and negatively buoyant starting jets, respectively, fitting equations can be obtained to predict the buoyant jet penetration rate. Based on these fitting equations, a revised circulation model is proposed by incorporating the effects of both over-pressure and buoyancy. The revised model is well consistent with the numerical results for all positively buoyant starting jets. However, for the negatively buoyant starting jets, this model can predict well only during the initial period. The over-pressure has little influence on the vortex ring characteristics of the starting jets with positive buoyancy, whereas it can significantly affect the vortex ring formation of the negatively buoyant starting jets at moderate Richardson numbers. As the positive Richardson number increases, the instabilities of the trailing shear layer occur earlier. At moderately negative Richardson numbers, a "double plume" structure (an inner sinking circular forced plume and an outer rising annular plume) can be observed. The outer negative vorticity layers develop gradually due to the baroclinic effect. Consequently, the size and strength of the leading vortex progressively decrease. As the negative Richardson number decreases, the negative vorticity layers occur earlier and grow faster.

I. INTRODUCTION

Vortex rings can be readily found in many flow features in nature as well as in many practical engineering applications: from volcanic eruptions[1] to the propulsive characteristics of some aquatic creatures.[2,3] The formation, evolution, and interaction of vortex rings have been the subject of numerous experimental, analytical, and numerical studies. One of the most important features about the vortex ring formation due to the roll-up of the separated shear layer is its disconnection from the generating mechanism at a critical dimensionless time $t^* = \overline{U}_0 t/D$ (where $\overline{U}_0$ is the time-averaged jet velocity and D is the jet exit diameter). This has imposed an upper limit to the growth of the leading vortex ring. This phenomenon was first observed experimentally and termed "vortex ring pinch-off" by Gharib *et al.*[4] They defined the critical value of the formation time as the "formation number" F and found that its value was in the range of 3.6–4.5 for the piston–cylinder mechanism. The determination of the formation number greatly depends on the definition of the dimensionless formation time t^*. Various definitions have been used in previous studies, but they were mainly applicable to the homogeneous starting flow (see the review of Dabiri[5]).

The circulation of the starting jet is a key parameter to characterize the formation process of the large scale vortical structure. For the homogeneous jet, several models have been proposed for determining its total circulation,[6,7] but the most common model used for the starting jet generated by a piston–cylinder mechanism is the so-called "slug model."[8] It is assumed that the starting jet possesses thin boundary layers so that the velocity is constant at the jet exit plane, approximately equal to the jet velocity U_0. Accordingly, the increase rate of the total circulation can be estimated as

$$\frac{d\Gamma_{sm}}{dt} = \frac{1}{2}U_0^2, \tag{1}$$

where the subscript "*sm*" denotes the slug-model prediction. Although the slug model has been used extensively owing to its simplicity, several experimental and numerical studies have demonstrated that the slug-flow model underpredicts the vortex ring circulation by up to 40%.[4,9,10] This may be in part due to the assumption that the flow at the jet exit is uniform and the transient start-up behavior and geometric differences in the vortex ring generators have been neglected.[11,12]

Several revised circulation models have also been developed but the disagreement remains. This is due largely to the parallel flow approximation that ignores the radial pressure gradients. The revised models also neglect the balance between the radial negative pressure gradients and centrifugal forces during the roll-up of the vortex sheet.[9] By considering the boundary layer growth, Shusser *et al.*[13] replaced the jet velocity U_0 in Eq. (1) by the velocity outside the boundary layer U_{ex}. Following this approach, Dabiri and Gharib[14] refined further the model for boundary layer growth within the cylinder and improved the accuracy of the model results. Another approach, developed by Krueger,[11] considers the effects of the over-pressure based on the integral of the incompressible vorticity transport equation over the domain external to the vortex ring generator. This provides two additional terms, which can be modeled using potential flow to account for the transient jet development and geometry differences. However, the model closure requires information about the trajectory of the vortex ring during formation.[12] Although above revised slug models improve the overall agreement with experimental measurements, they may not be applicable to the situation of starting buoyant jets with source-ambient density difference.

In practice, the starting buoyant jet with comparable initial momentum and buoyancy fluxes is a more common configuration for vortex formation. The effect of buoyancy on the starting jet dynamics is generally characterized by the dimensionless Richardson number. Wang *et al.* performed large eddy simulations on the behavior of the formation process of vortex rings in starting buoyant jets with both positive ($Ri_d \le 0.14$)[15] and negative ($Ri_d \ge -0.35$)[16] Richardson numbers. Here, $Ri_d = (\pi/4)^{1/2} g' D/U_0^2$ is the directional Richardson number, $g' = g\Delta\rho/\rho_a$ is the reduced gravity, $\Delta\rho = \rho_j - \rho_a$ is the density difference between the jet and ambient fluid, and g is the gravitational acceleration. However, they did not identify the formation number for $Ri_d \le -0.05$ (denoted hereafter as the regime of moderate buoyancy effects) due to limitations in the procedure they used to detect the vortex pinch-off event.[16] Marugán-Cruz *et al.*[17] studied the formation of vortex rings in negatively buoyant starting jets in the regimes of weak to moderate buoyancy effects, occurring at $0 \ge Ri \ge -0.2$, where the Richardson number is defined as $Ri = g'D/U_0^2$. The formation regimes of vortex rings in starting forced plume, with low Richardson numbers in the range of $-0.06 \le Ri \le 0.06$, were also studied numerically by Gao and Yu.[18]

Theoretically, Wang *et al.*[15,16] proposed a revised model of circulation, impulse, and kinetic energy for starting buoyant jets by linearly combining the initial momentum and buoyancy fluxes. They assumed that the discharged fluid rolls up to form a vortex ring and half of its surface is exposed to the ambient quiescent fluid. The model is found to be applicable for weakly negatively buoyant jets ($Ri_d > -0.05$) but it fails for strongly negatively buoyant jets ($Ri_d < -0.05$).[16] Based on the general formation time definition of Dabiri,[5] Gao *et al.*[19] derived a revised definition of the formation time and circulation model for both starting jets and starting forced plumes. However, the validity of the revised buoyant formation time was demonstrated only for the low Richardson number cases ($-0.1 \le Ri \le 0.1$). Hence, a revised circulation model should be proposed and examined for starting buoyant jets at moderate Richardson numbers.

In this paper, we intend to elucidate the vortex ring formation dynamics in positively and negatively buoyant starting jets at moderate Richardson numbers $0.06 < |Ri| \le 0.321$ using the theory and numerical method. The rest of the paper is organized in the following way. We first derive a new circulation model for starting buoyant jets by considering the effects of buoyancy, over-pressure, and boundary layer growth in Sec. II. Second, the details of the problem description and the numerical method on vortex ring formation are introduced in Sec. III for the axisymmetric starting buoyant jet with positive and negative buoyancy. In Sec. IV, the theoretical models and numerical results are compared in terms of characteristic kinematic and dynamic parameters (such as circulation and jet penetration height). By adopting the revised circulation method, the effects of the Richardson number on the formation number are identified and discussed. The paper ends with brief concluding remarks in Sec. V.

II. TOTAL CIRCULATION IN STARTING BUOYANT JETS

The starting buoyant jet not only is driven by momentum, but also is subjected to the influence of the reduced gravity as a result of temperature/concentration differences. Here, only the concentration difference, i.e., a lighter or heavier fluid released into a different ambient fluid, is considered. It is also well established that the formation of vortex rings is mainly an inviscid process for $Re \ge 2000$.[20,21] Following Krueger[11] and Iglesias *et al.*,[22] the circulation equation for the starting buoyant jet can be obtained by deriving the vorticity transport equation. The vorticity equation for the incompressible baroclinic fluid in a control volume under the action of conservative external body force can be written as

$$\frac{\partial \boldsymbol{\omega}}{\partial t} = -\nabla \times (\boldsymbol{\omega} \times \boldsymbol{u}) + \frac{1}{\rho^2}(\nabla\rho \times \nabla p), \tag{2}$$

where the bolded symbols indicate that the quantities are vectors. Integrating Eq. (2) over a control surface S with bounding the contour C of the control volume gives

$$\frac{\partial \Gamma}{\partial t} = \underbrace{-\oint_C (\boldsymbol{\omega} \times \boldsymbol{u}) \cdot d\boldsymbol{c}}_{\partial\Gamma_f/\partial t} + \underbrace{\oint_C \frac{1}{\rho^2}(\nabla\rho \times \nabla p) \cdot d\boldsymbol{s}}_{\partial\Gamma_b/\partial t}. \tag{3}$$

The first terms on the right-hand side $\partial\Gamma_f/\partial t$ is the increase rate of the total circulation, which is produced by the vorticity flux through the jet exit plane and the second term $\partial\Gamma_b/\partial t$ is the rate of the baroclinic circulation production.

Following the analysis of Krueger[11] for the homogeneous starting jet, integrating the term $\partial\Gamma_f/\partial t$ on the right side of Eq. (3) over time provides

$$\Gamma_f = \underbrace{\frac{1}{2}U_{cl}^2 t}_{\Gamma_U} + \underbrace{\int_0^{\infty}\int_0^{D/2} u\frac{\partial v}{\partial x} dr dt}_{\Gamma_p}, \tag{4}$$

where U_{cl} is the axial velocity at the center of the jet exit plane, i.e., $(x, r) = (0, 0)$. The first term Γ_U in Eq. (4) corresponds to the vorticity flux under the parallel flow approximation, i.e., the radial velocity v is zero. Due to the boundary layer growth at the inner surface of the cylindrical nozzle during fluid ejection, the centerline velocity is assumed to equal the velocity outside the boundary layer at the jet exit plane, which is given by Dabiri and Gharib[14] as

$$U_{cl} = U_{ex} = U_0\left(1 + \frac{8}{\sqrt{\pi}}\frac{1}{\sqrt{Re}}\sqrt{\frac{U_0 t}{D}}\right). \tag{5}$$

It is noted that the first term on the right-hand side of Eq. (4) is equivalent to the slug model if the boundary layer correction is not considered, namely $U_{ex} = U_0$ and $\Gamma_U = \Gamma_{sm}$. The second term Γ_p on the right-hand side of Eq. (4), i.e., the vorticity flux due to the axial gradients in the radial velocity, is associated with the over-pressure at the jet exit plane. For the starting jet with nearly impulsive velocity program, the over-pressure contribution to the total circulation Γ_p can be determined by integrating the unsteady Bernoulli equation for the potential flow solution in front of a translating disk,[11]

$$\Gamma_p \approx \frac{U_0 D}{C_p}, \tag{6}$$

where C_p is the geometric constant, which is found to be equal to π for the tube nozzle configuration and equal to 2 for the orifice nozzle configuration. Substituting Eqs. (5) and (6) into Eq. (4), we obtain a revised circulation model for the homogeneous starting jet.

Iglesias *et al.*[22] had pointed out that the baroclinic circulation generation mainly occurs across the source-ambient fluid interface along the trailing jet and leading vortex ring for high Reynolds number and Schmidt number. Following Gao *et al.*,[19] the last term in Eq. (3) can be obtained as

$$\frac{\partial \Gamma_b}{\partial t} = g' x_f, \tag{7}$$

where x_f, a function of time, denotes the streamwise penetration of the jet front. It is noted that the reduced gravity g' is negative for the negatively buoyant jet.

Finally, by considering the contributions from the jet discharged velocity, boundary layer growth, over-pressure and buoyancy, and assuming that the buoyant starting jet is initiated impulsively, the total circulation Γ_t of the starting buoyant jet can be obtained as

$$\Gamma_t = \underbrace{\frac{1}{2}U_{ex}^2 t}_{\Gamma_U} + \underbrace{\frac{U_0 D}{C_p}}_{\Gamma_p} + \underbrace{\int_0^t g' x_f dt}_{\Gamma_b}. \tag{8}$$

III. NUMERICAL METHOD AND SETUP

Vortex ring formation was studied numerically by solving the axisymmetric, time dependent incompressible Navier–Stokes equations, together with the species equation. The energy equation was not solved since the simulations were performed at constant temperature. The equations were discretized on the domains with the coordinate systems as shown in Fig. 1. The geometry is axisymmetric, therefore, only the x–r plane is considered. The domain dimensions in the x–r plane were chosen to be $40D$ in length and $15D$ in height to ensure a negligible domain size effect on the flow evolution ($D = 0.6$ cm is the jet exit diameter). The jet fluid with different density was injected downward into the static ambient fluid through a circular orifice nozzle. The average velocity at the nozzle exit is 0.0605 m/s, and the Reynolds number is $Re = 570$. When the heavier fluid was injected downward into the ambient fluid ($\rho_j > \rho_a$), the buoyancy force and momentum fluxes were aligned in the same direction (reduced gravity $g' > 0$), a positively buoyant jet was formed, whereas a negatively buoyant jet was formed if the lighter fluid was injected downward into the ambient fluid ($\rho_j < \rho_a$, $g' < 0$). A summary of the flow parameters for different cases in this study is presented in Table I.

The governing equations were discretized using the finite volume approach implemented by the commercial computational fluid

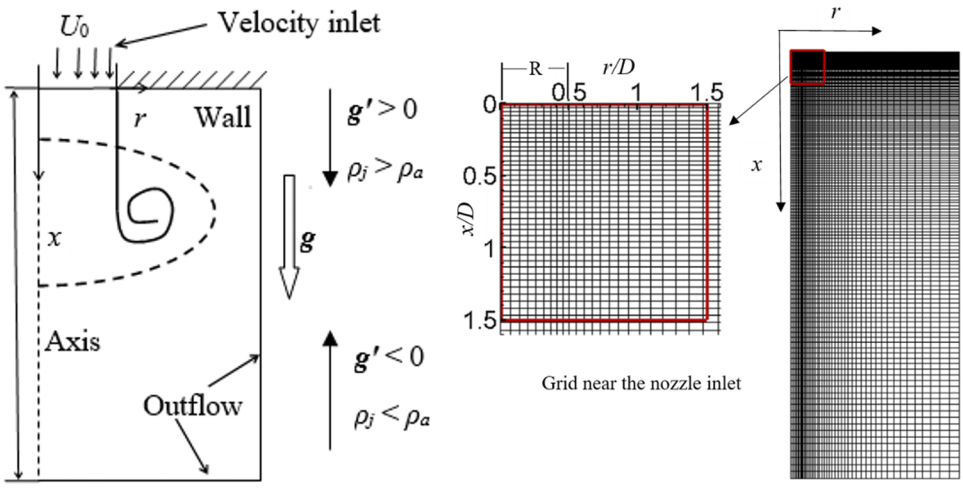

FIG. 1. (a) Computational domain (not to scale) and boundary conditions and (b) distribution of the grid adopted for the numerical study, with an enlarged view near the jet exit region (only every fifth mesh point is shown).

TABLE I. Summary of simulation parameters and formation numbers F for the starting buoyant jets.

Case	N5	N4	N3	N2	N1	H0	P1	P2	P3	P4
$\Delta\rho/\rho_a$	−0.02	−0.015	−0.011	−0.0085	−0.005	0	0.005	0.01	0.014	0.02
Ri	−0.321	−0.245	−0.18	−0.133	−0.080	0	0.080	0.161	0.226	0.321
F	...	1.3	1.9	2.5	2.8	4.2	5.0	5.5	6.5	7.0

dynamics (CFD) package (Ansys Fluent 2019 R1). The convective terms were discretized using the QUICK scheme and the pressure–velocity coupling was implemented using the SIMPLEC algorithm. The governing equations were solved in a segregated manner using an implicit, second-order time dependent formulation. Boussinesq approximation, under which the density variations can be neglected in all but the body force terms, was used here due to the small density difference in the current study. The mass diffusivity between the jet fluid and ambient fluid was taken as a constant.

As shown in Fig. 1(a), the flow axisymmetry was imposed along the jet centerline. The velocity inlet condition was imposed at the jet exit. The downstream and lateral boundaries were specified as free outflow conditions, where flow properties were extrapolated from the interior. No slip and zero mass diffusion conditions were imposed at the upper boundary (wall). At the start of the calculations, the flow velocities and jet mass fraction were zero throughout the computational domain, except at the nozzle inlet where the jet mass fraction was unity and the axial velocity profile pertained to fully developed laminar flow. The domain was discretized using a non-uniform, rectangular grid with higher node density near the jet exit and shear layer region (i.e., $x/D = 0$ and $r/D = 0.5$) in order to resolve the areas of large velocity and concentration gradients [see Fig. 1(b)]. To test the grid independence, case N1 with $Ri = 0.080$ was simulated with three grids having nodal dimensions 800 × 120, 1000 × 200, and 1200 × 280. Comparing Γ_t for the three cases gave less than 3% difference between the 1000 × 200 and 1200 × 280 grids for both geometries. Thus, the 1000 × 200 grid was used to obtain the results for this numerical investigation. Moreover, in order to validate the numerical method, the results of the jet front penetration, which are of great interest in the present study as suggested by Eq. (7), are compared with the numerical results of Wang *et al.*[16,23] for cases at similar Richardson numbers in Fig. 2. Note that the technique of identifying the jet front position will be introduced in Sec. IV B. As shown, the current results are in good agreement with those for the positively and negatively buoyant jets studied by Wang *et al.*[16,23] (see Fig. 9 in Ref. 23 and Fig. 3 in Ref. 16, respectively), especially for the positively buoyant cases.

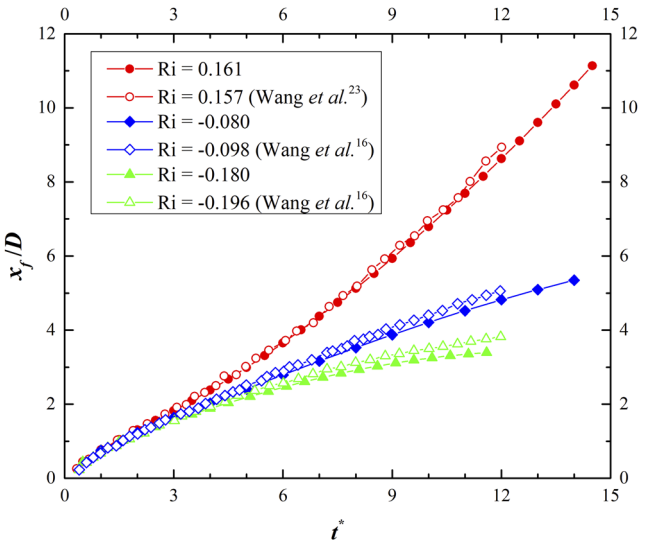

FIG. 2. The evolution of the jet front penetration for starting buoyant jets at three Richardson numbers. The current numerical result is compared with the existing results of Wang *et al.*[16,23]

IV. RESULTS AND DISCUSSIONS

A. Flow development of starting buoyant jets

The mass fraction and dimensionless vorticity $\omega^* = \omega D/U_0$ contours for the five starting buoyant jets at different Richardson numbers are shown in Fig. 3. The contours are presented against the non-dimensional time $t^* = tU_0/D$. Except for $Ri = -0.321$, the formation of the vortex head for all cases can be observed and the vortex ring has an initial round shape. However, its shape changes gradually under the influence of both vorticity influx from the source and baroclinic production of vorticity. Comparing to the results obtained by Marugán-Cruz *et al.*[24] and Gao and Yu,[18] the flow structures are similar at the initial stage ($t^* < 5$) indicating that the buoyancy effects on the flow dynamics are insignificant. In addition, the vorticity is maximum at the jet exit due to the presence of thin shear layers and the vorticity levels decrease downstream of the inlet due to viscous diffusion.

For weaker positively buoyant cases such as $Ri = 0.161$ [case P2, Fig. 3(a)], the formation of the leading vortex and the secondary instabilities in the trailing shear layer can be observed as the leading vortex moves downward. At $t^* = 8.5$, the vortex ring starts to detach from the trailing shear layer because the vorticity layer connecting the leading vortex shrinks. The diameter of the vortex ring becomes larger, and a weak initial trailing vortex can be distinguished in the trailing shear layer at $t^* = 15$. As Ri increases to 0.321 [case P4, Fig. 3(b)], the separation of the leading vortex is found to occur later ($t^* = 15.5$), while the instabilities of the trailing shear layer develop earlier ($t^* < 13.5$) due to larger positive buoyancy acceleration. The strength of the secondary vortex in the trailing jet is also larger than that in the P2 case. It is also observed that the entrainment of the secondary vortices and more concentrated distribution of vortices are found in the trailing jet after $t^* = 13.5$. For higher values of Ri, the

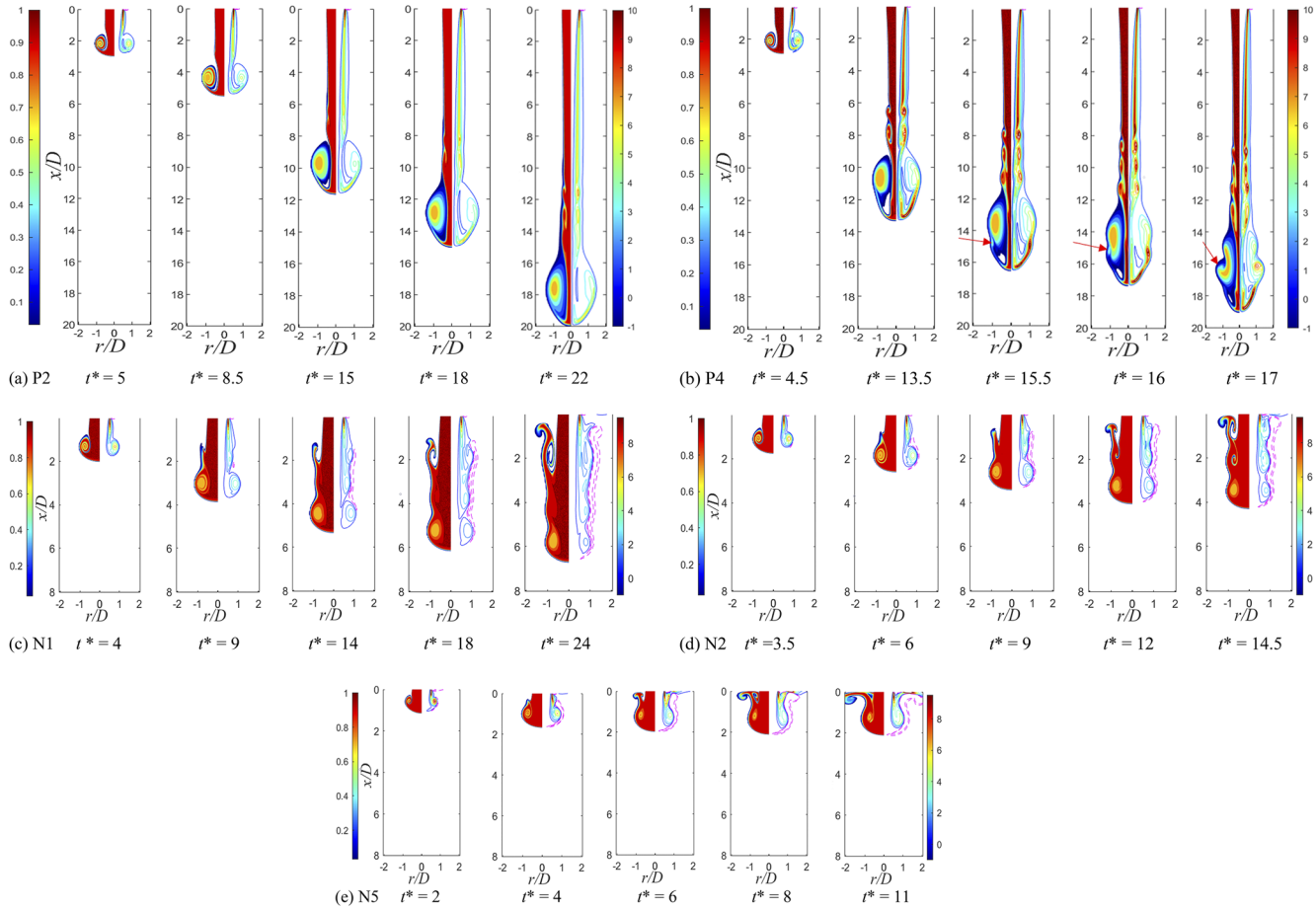

FIG. 3. The evolution of the jet mass fraction (left) and vorticity (right) contours for starting buoyant jets with different *Ri* against nondimensional formation time t^*: (a) P2, *Ri* = 0.161; (b) P4, *Ri* = 0.321; (c) N1, *Ri* = −0.080; (d) N2, *Ri* = −0.133; and (e) N5, *Ri* = −0.321. The pink dashed lines indicate the negative vorticity levels.

trailing shear layer is more unstable and, thus, it is more susceptible to Kelvin–Helmholtz instability and the associated secondary vortex roll-up. The development of the secondary vortex, ahead of the trailing jet, will accelerate the instability of the leading vortex ring. As pointed by the red arrows in Fig. 3(b), a high vorticity zone (or mass fraction) is generated in the shear layer in front of the leading vortex at $t^* = 15.5$. Then, as time evolves, this small-scale structure is gradually entrained by the leading vortex ring core and has a direct interaction with the latter. As shown at $t^* = 17$, the mass fraction distribution of the leading vortex displays a crescent shape rather than elliptic, which is also observed in the recent study of the positively buoyant vortex ring formation.[25] As a result, the leading vortex ring core becomes more disturbed and less coherent. Therefore, it can be concluded that, due to the small-scale vortices being entrained into the leading vortex ring core, the incoherent process of the vortex ring is accelerated in the case of a larger Richardson number (*Ri* = 0.321). It should be noted that our observation is similar to the results reported by Li *et al.*[26]

As the negative Richardson number decreases (cases N1 and N2), the leading vortex ring translates at a slower rate and its detachment from the trailing jet occurs earlier [Figs. 3(c) and 3(d)]. In addition, a negative vorticity region forms outside the leading vortex ring and the trailing shear layer. This is consistent with the observation of Marugán-Cruz *et al.*[24] and Gao and Yu.[18] As shown in Fig. 3(c) for case N1, the initial generation of a vorticity layer of negative sign is at the trailing shear layer and close to the rear boundary of the leading vortex ($t^* = 9$). As the Richardson number decreases to *Ri* = −0.133 [N2 in Fig. 3(d)], the negative vorticity layer occurs earlier ($t^* = 3.5$) and develops faster. However, it appears outside of the leading vortex ring, not just around the trailing shear layer. Since this layer mainly contains fluids of density lower than that of the ambient fluids, it would be pushed upward by the buoyancy forces until it eventually reaches the top wall, forming the annular reverse flow around the inner downward jet. This flow structure has been termed previously as a "double plume."[27] On the other hand, as time evolves, owing to the negative vorticity engulfing the leading vortex, the size and strength of the leading vortex gradually decrease [see $t^* = 24$ in Fig. 3(c) and $t^* = 14.5$ in Fig. 3(d)]. From the mass fraction contours on the left-hand side of each figure, there exist maximum density gradient zones, which

correspond to the regions of negative vorticity production due to the baroclinic effect. At large formation times, the reverse flow can be divided into two parts. One part turns radially outward, while the other part moves inwards and entrains the ambient fluids to evolve into a coherent structure [$t^* = 24$ for N1 in Fig. 3(c) and $t^* = 14.5$ for N2 in Fig. 3(d)]. Finally, case N5 ($Ri = -0.321$) is shown in Fig. 3(e). The negative vorticity layer can be identified at an earlier stage so that the leading vortex has a less time to fully develop. This is consistent with the observation of Wang *et al.*[16] that the pinch-off process does not exist for $Ri < -0.226$ where the leading vortex and jet stem remain connected at all time.

B. Jet front penetration and the leading vortex ring boundary

To evaluate the kinematics of the starting buoyant jet at moderate Richardson numbers, its front penetration characteristics are examined next. The front boundary of the starting buoyant jet edge x_f can be identified as the location where the density difference is 3% of its initial value.[28] It is noted that x_f is also used as the front boundary of the leading vortex ring. As shown in Fig. 4, the position of the jet front increases monotonically, and the rate of increase grows very rapidly with increasing Richardson number.

Consistent with the results of flow evolution (Fig. 3), at short times (i.e., for $t^* \le 5$ and $t^* \le 3$ as pointed by the red arrows for the positively and negatively buoyant starting jets, respectively), the jet front position x_f does not depend on the Richardson number, indicating that buoyancy effects are nearly negligible initially. This phase was referred to as the initial overlapped phase.[23] After that, the effect of the buoyant acceleration/deceleration becomes appreciable for the positively buoyant jet and negatively buoyant jet, respectively. With the increase in Richardson numbers for the positively buoyant cases [Fig. 4(a)], the jet front position increases more rapidly with time. On the other hand, a steady state is reached for smaller negative Richardson numbers, $Ri \le -0.080$, for which the final penetration depth remains constant. For $Ri = -0.321$, the jet front can reach a steady position in shorter time such that the leading vortex cannot be fully developed [see also Fig. 3(e)].

As shown in Fig. 4, the developments of the jet front are not self-similar for different Richardson numbers. To scale the penetration depth, many researchers used the function of the initial volume flux Q, momentum flux M, and buoyancy flux B as similarity variables.[23,29,30] For example, Wang *et al.*[23] scaled the penetration height with $Q^{1/5}M^{1/2}/B^{2/5}$ and the time as $tQ^{4/5}/B^{3/5}$. In addition, Marugán-Cruz *et al.*[24] used the Froude number, which is defined as $Fr = U_0^2/g'D$, to scale the vortex core position. Similarly, to obtain a self-similarity equation of the penetration depth of the starting buoyant jets for different Richardson numbers, we scale the penetration depth with the Richardson number. Since the trajectories of the jet front are different for positively and negatively buoyant jets, the dimensionless penetration height x_f/D is scaled as $|Ri|x_f/D$ and $|Ri|^{2/5}x_f/D$ for positively and negatively buoyant jets, respectively. The physical time is scaled as $|Ri|t^*$ for all the cases studied. The time history of the jet penetration height for starting buoyant jets with different Richardson numbers is shown in Fig. 5. The data collapse onto a single curve, especially for the positively buoyant jets. It suggests that $|Ri|x_f/D$ or $|Ri|^{2/5}x_f/D$ and $|Ri|t^*$ are the appropriate similarity variables and the relation is independent of the Richardson number. Hence, a reasonable fit can be obtained for the positively buoyant jets:

$$|Ri|\frac{x_f}{D} = 0.1205(|Ri|t^*)^2 + 0.458|Ri|t^* + 0.05$$

or

$$x_f = 12.047D|Ri|t^2 + 4.58Dt + 0.05D/|Ri| \quad (9)$$

and for the negatively buoyant jets:

$$|Ri|^{2/5}\frac{x_f}{D} = -0.3198(|Ri|t^*)^2 + 1.553|Ri|t^* + 0.1296$$

or

$$x_f = -31.98D|Ri|^{8/5}t^2 + 15.53D|Ri|^{3/5}t + 0.1296D/|Ri|^{2/5}. \quad (10)$$

Another important feature associated with the kinematics of the forming buoyant vortex ring is its boundary with the trailing jet stem x_{rb}, which delineates the rear boundary of the vortex ring. There are several different methods reported in the literature to

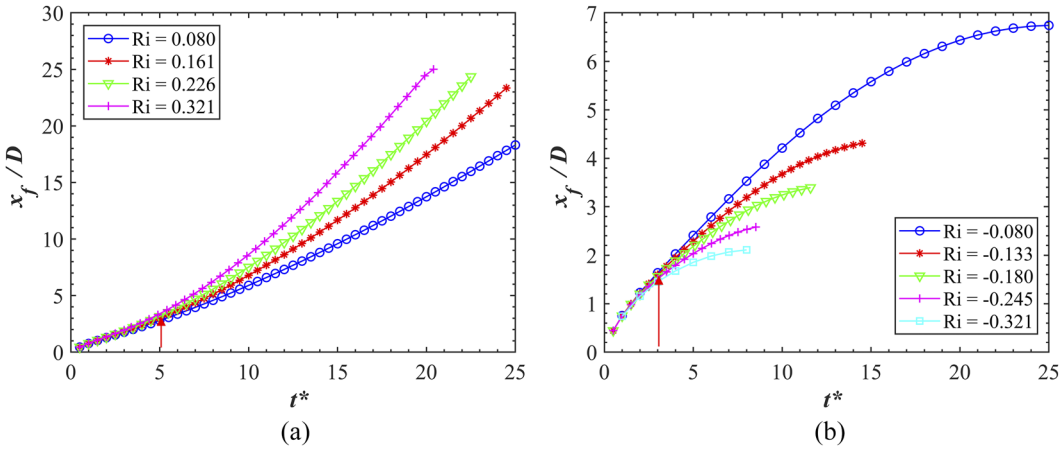

FIG. 4. The evolution of the jet front, x_f/D with dimensionless time t^*, for the starting buoyant jet at (a) positive Richardson number and (b) negative Richardson number.

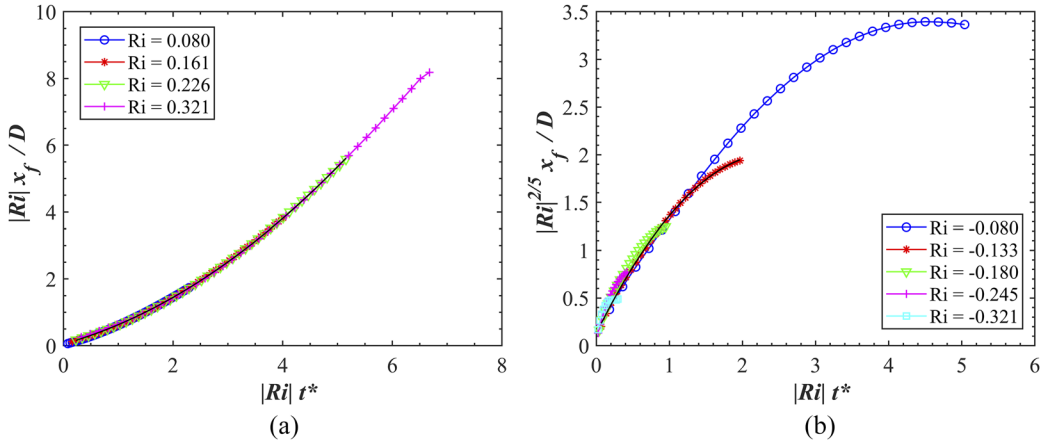

FIG. 5. The jet front, x_f/D, as a function of time using similarity variables for the starting buoyant jets at (a) positive Richardson number and (b) negative Richardson number.

identify the vortex boundaries.[4,15–18,24] Wang *et al.*[15,16] employed the minimum value in the integrated vorticity $I_\omega = \int_0^\infty \omega dr$ as the boundary between the leading vortex region and the trailing jet region throughout the vortex ring formation process. However, this integrated vorticity I_ω could be affected by the event of the trailing vortex entrainment. To eliminate the influence of the vortex engulfment of I_ω, Gao and Yu[18] integrated the vorticity radially from $D/2$ to the infinite as

$$I_{\omega R} = \int_{D/2}^{\infty} \omega dr, \tag{11}$$

and defined its minimum as the rear boundary of the leading vortex ring. Therefore, we adopted the method of Gao and Yu[18] for the vortex rear boundary detection. As shown in Figs. 6(a) and 6(b), the axial positions at the minimum of the integration $I_{\omega R}$ correspond to the rear boundary of the leading vortex ring. The evolution of the normalized rear boundary x_{rb}/D against t^* for different Richardson numbers is presented in Fig. 6(c). Similar to the jet front position, the rear boundary x_{rb}/D grows very rapidly with time and the rate of increase becomes larger with Ri for positively buoyant jets, but the change of the rear boundary x_{rb}/D for negatively buoyant jets is reverse.

C. Circulation and formation number

In this section, we discuss the evaluation of the dimensionless circulation $\Gamma^* = \Gamma/(U_0 D)$ with the formation time t^* and predict the formation number for the starting buoyant jet at moderate

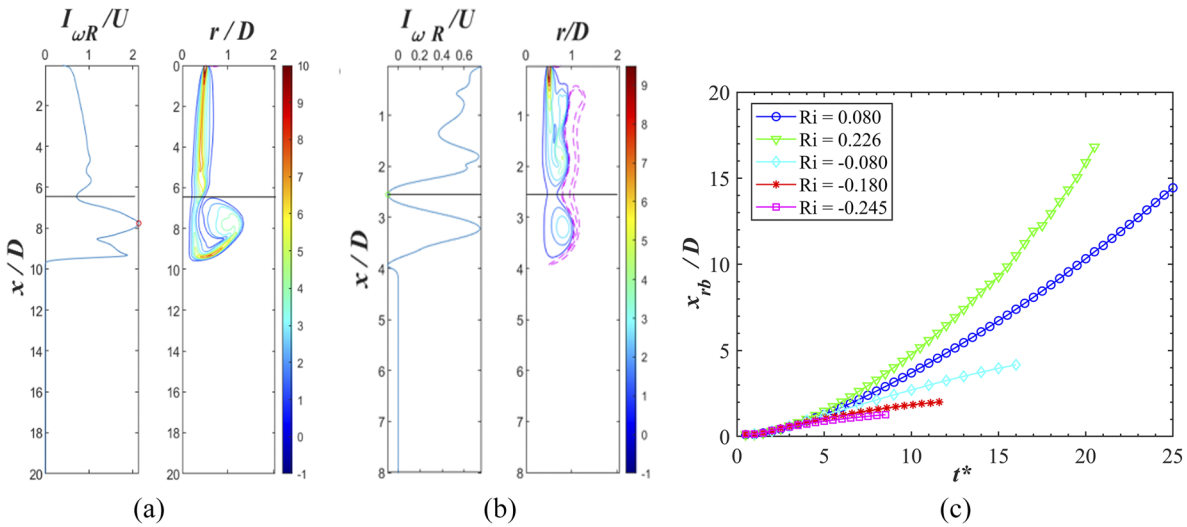

FIG. 6. The axial distribution of the $I_{\omega R}$ and vortex contour at $t^* = 12$ for (a) case P3 ($Ri = 0.226$); (b) case N2 ($Ri = -0.133$); (c) the evolution of the dimensionless rear boundary x_{rb}/D against t^* for different Richardson numbers. The black lines in Figs. 5(a) and 5(b) indicate the rear boundaries of the vortex ring.

Richardson numbers. As discussed in Sec. II, the total circulation Γ_t in a starting buoyant jet, given by Eq. (8), is a combination of the contributions from the vorticity flux contribution Γ_f at the jet exit plane and the baroclinic production of vorticity Γ_b within the entire jet wake region. The prediction of the vorticity flux term Γ_f is mainly based on the revision of the slug model, which includes the effects of boundary layer growth and over-pressure. As suggested by Eq. (7), the baroclinic circulation Γ_b is dependent on the prediction of the jet front penetration x_f. For the starting buoyant jets with low Richardson numbers ($-0.1 < Ri < 0.1$), it is appropriate to approximate that the buoyant jet front penetrates at a constant velocity, which is only proportional to the jet velocity U_0,[19,24] i.e., $x_f = U_0 t/2$. Therefore, for these cases ($-0.1 < Ri < 0.1$), the buoyancy circulation Γ_b can be written as

$$\Gamma_b = \int_0^{t_p} g' x_f dt = \frac{1}{4} U_0 g' t^2. \tag{12}$$

In this study of moderate Richardson numbers, we will use the time integral of the product of the fitted equation of the jet front penetration x_f [i.e., substituting Eqs. (9) and (10) into Eq. (8)] to estimate the baroclinic circulation.

To study the effects of over-pressure and the baroclinic vorticity production, three models are compared with the numerical results for starting buoyant jets (see Table II). Here, we consider the nozzle as the tube geometry; hence, $C_p = \pi$ is employed in the over-pressure circulation.[11] The effect of the over-pressure can be obtained by comparing models 1 and 2, and the different buoyant circulation modeling can be compared by examining the prediction of models 2 and 3.

To test the accuracy of the current model [Eq. (8)], the numerical results of the dimensionless circulation $\Gamma^* = \Gamma/(U_0 D)$ with different Richardson numbers are compared with the results of the three models against the formation time t^*, as shown in Fig. 7. For the positively buoyant jets [Figs. 7(a) and 7(b)], the effect of the over-pressure is barely appreciable by comparing the results from models 1 and 2. Hence, the over-pressure can be regarded as negligible. For smaller positive Richardson number $Ri = 0.08$ (case P1), the results for the three models and simulation are in good agreement, especially for model 3. As the Richardson number increases [see Fig. 7(b)], models 1 and 2 underestimate the total circulation of the starting buoyant jet, while model 3 still matches closely the present numerical results. As shown in Figs. 7(a) and 7(b), model 3 is well consistent with the numerical results for all positive Richardson number cases. Therefore, the time integral of the fitted equation for the jet front x_f [Eq. (9)] can estimate appropriately the baroclinic circulation Γ_b. This also demonstrates the validity of Eq. (8) for positively buoyant starting jets, i.e., the total circulation can be treated as a linear combination of the flux circulation due to the jet exit axial velocity and buoyant circulation due to the baroclinic production.

In contrast to the positively buoyant jets, the effect of the over-pressure is relatively large and increases gradually with the decrease in the negative Richardson number [Figs. 7(c)–7(f)]. All three models cannot predict well the total jet circulation. Model 1 underestimates greatly the numerical results for all negative Richardson number cases. It is also noted that models 2 and/or 3 with the over-pressure correction can predict the numerical results well just during the initial period. For the larger negative Richardson number $Ri = -0.08$ and -0.133 [Figs. 7(c) and 7(d)], the estimation by model 3 is still in good agreement with the numerical results. However, as the negative Richardson number decreases ($Ri = -0.18$ and -0.245), model 3 deviates and underestimates dramatically the numerical results while model 2 can predict better at the initial time stage [Figs. 7(e) and 7(f)]. This maybe because the effect of the negative buoyancy increases with the decrease in the negative Richardson number. By comparing Figs. 3(c) and 3(d) with Figs. 7(c) and 7(d), it is found that models 2 and 3 start gradually to deviate from the numerical results as the reverse flow occurs. When the negative Richardson number decreases, the reverse flow occurs early. Consequently, the deviating time of models 2 and 3 [pointed by the black arrows in Figs. 7(c)–7(f)] occurs early. As shown in Figs. 7(c)–7(f), with time proceeding, all three models underestimate dramatically the numerical prediction due to the increase in the negative vorticity layers. Therefore, the decoupling circulation model (see Sec. II) may be not suitable to the starting buoyant jets at moderate negative Richardson numbers. In addition, for negatively buoyant jets, when the buoyancy effect becomes dominant, the flow structure develops into a "double plume" (an inner sinking circular forced plume and an outer rising annular plume)[23] [see also Figs. 2(c)–2(e)], whose influence is not included in the current model [Eq. (8)]. Therefore, a piecewise expression for the model may offer better prediction for the negatively buoyant jets, which will be considered in the future.

Besides the total circulation of the starting buoyant jet, the evolution of vortex ring circulation for the cases with different Richardson numbers is also presented in Fig. 7. It is noted that the vortex ring circulation is obtained by integrating the vorticity within the vortex ring region, which is delineated by its axial boundary,

TABLE II. Three total circulation models for the starting buoyant jets.

Model	Equations
Model 1 [buoyant circulation in Eq. (12)]	$\Gamma_{t\_h} = \frac{1}{2} U_{ex}^2 t + \frac{1}{4} U_0 g' t^2$
Model 2 {the effects of the buoyancy [Eq. (12)] and over-pressure [Eq. (6)]}	$\Gamma_{t\_b1} = \frac{1}{2} U_{ex}^2 t + \frac{U_0 D}{\pi} + \frac{1}{4} U_0 g' t^2$
Model 3 [buoyant circulations are the time integral of Eqs. (9) and (10) for the positive and negative Ri, respectively]	$\Gamma_{t\_b2} = \frac{1}{2} U_{ex}^2 t + \frac{U_0 D}{\pi} + \int_0^t g' x_f dt$

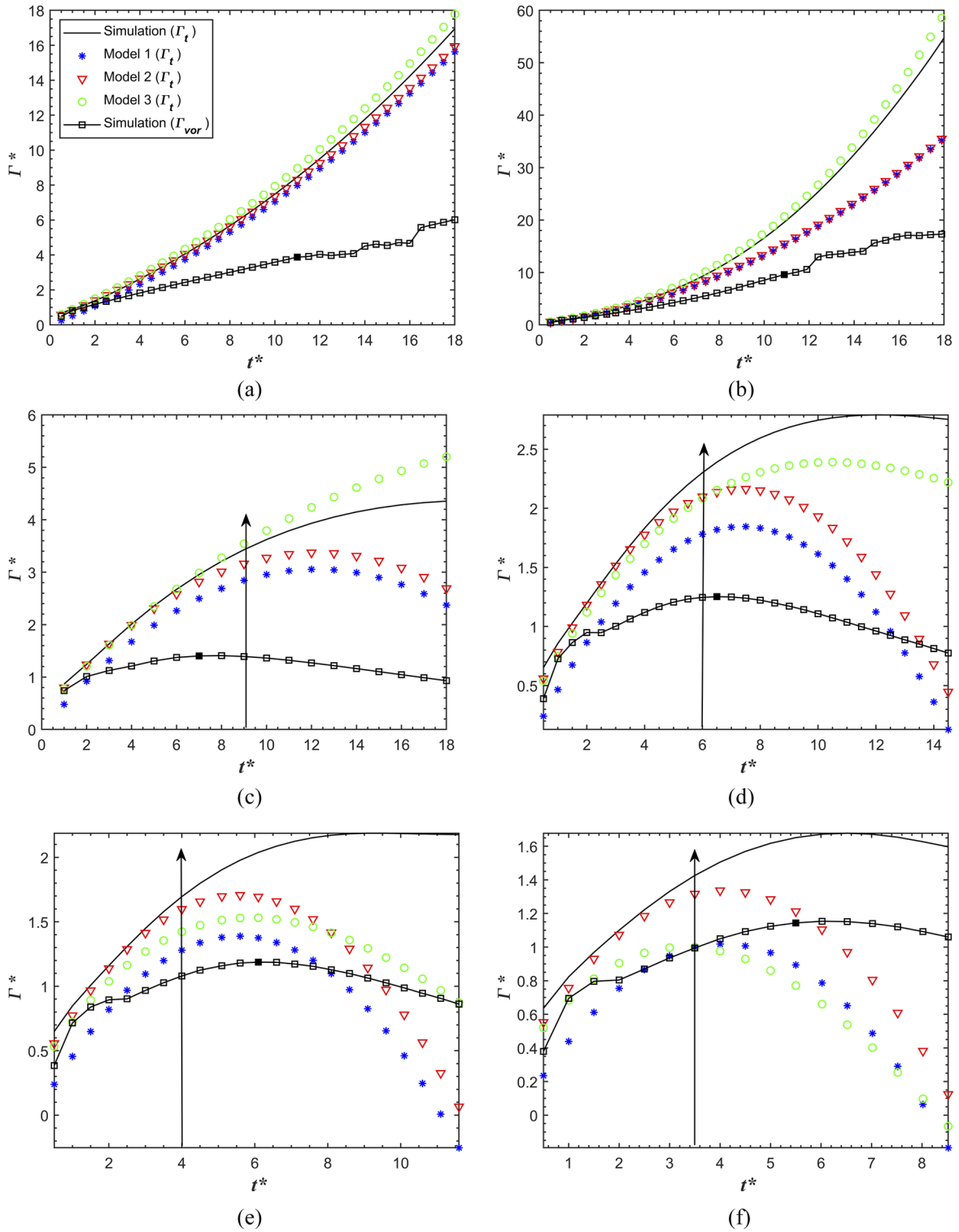

FIG. 7. The variation of dimensionless circulation for the total starting buoyant jet Γ_t and the leading vortex ring Γ_{vor} against the formation time t^* at different Richardson numbers: (a) $Ri = 0.08$, (b) $Ri = 0.321$, (c) $Ri = -0.08$, (d) $Ri = -0.133$, (e) $Ri = -0.18$, and (f) $Ri = -0.245$. The positions of the line arrows indicate the moment at which the results of models 2 or 3 start to deviate from the numerical results.

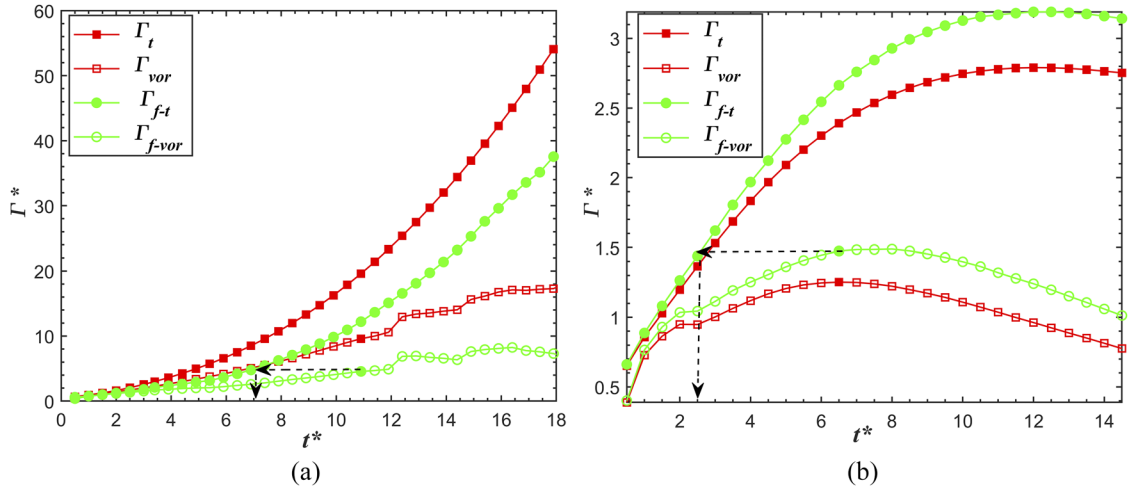

FIG. 8. The evolution of the total and source part of the jet and vortex circulation against the formation number for (a) case P4 (Ri = 0.321) and (b) case N2 (Ri = −0.133). The larger red solid square and green solid circular symbols indicate the total and source part of the vortex circulation at the separation time, respectively. The arrows with dashed lines show the procedure of determining the formation number.

i.e., x_f and x_{rb}, as shown in Figs. 4 and 6(c). For the negatively buoyant jets, only positive vorticity in the vortex ring area is computed.[14] As shown in Fig. 7, the vortex ring circulation Γ_{vor} can continue to increase for positively buoyant starting jets during its long-term development [Figs. 7(a) and 7(b)] while it decreases gradually for negatively buoyant starting jets [Figs. 7(c)–7(f)] due to the vorticity cancellation with the outside negative vorticity layers [see also Figs. 3(c) and 3(d)].

Once the total circulation and vortex ring circulation of the starting buoyant jets are obtained, we can proceed to identify the critical time scale for the vortex ring formation, i.e., the formation number F. For the starting buoyant jets, the classic circulation method of Gharib *et al.*[4] cannot be used directly since a part of the vortex ring circulation stems from the baroclinic production of vorticity within the vortex ring area, not entirely from the vorticity flux by the trailing shear layer. To eliminate the influence of baroclinic vorticity production, Gao and Yu[18] proposes a modified circulation method for identifying the buoyant formation number by distinguishing the circulation from the jet source and that from baroclinic production, i.e., only the flux circulation, Γ_f, was considered in determining the formation number. As discussed in Sec. II, the flux circulation Γ_f of the starting buoyant jet can be obtained from the difference between the total circulation and the buoyance circulation, i.e., $\Gamma_f = \Gamma_t - \Gamma_b$. Similarly, by applying this idea to the leading vortex ring, the flux vortex circulation, Γ_{f_vor}, is computed as $\Gamma_{f\_vor} = \Gamma_{vor} - \Gamma_{b\_vor}$. Here, the buoyancy (vortex) circulation Γ_b (Γ_{b_vor}) can be obtained via the temporal integral of the second term on the right-hand side of Eq. (3). In addition, following Gao and Yu,[18] the separation time τ can be determined as the critical formation time at which the vorticity flux from the trailing shear layer into the leading vortex ring vanishes, i.e., the disconnection of these two flow structures. Once the separation time is found, the formation number F is calculated as the dimensionless formation time at which the flux term of the total circulation matches that of the leading vortex ring at the separation time, i.e., $\Gamma_f(F) = \Gamma_{f\_vor}(\tau)$. The computation procedure is illustrated in Fig. 8 by the black arrows with dashed lines.

The formation numbers F for all cases studied (except for case N5 with Ri = −0.321 where the vortex ring pinch-off never occurs) are presented in Fig. 9 and summarized in Table I. It can be observed that the formation number increases monotonically with the Richardson number. The numerical results of the formation number reported in the literature[16–18] are also

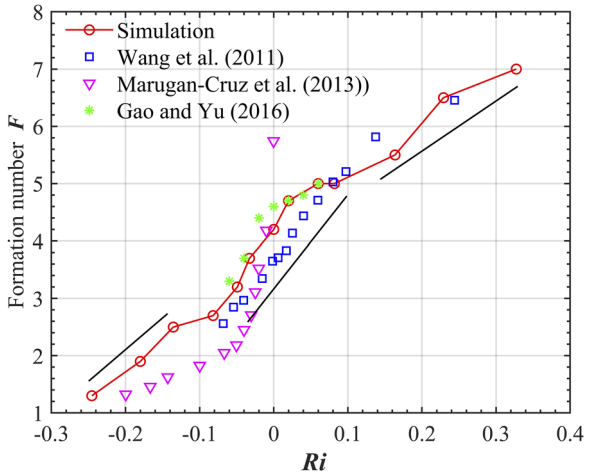

FIG. 9. The variation of the critical formation number F against the Richardson number in the range $-0.321 < Ri \leq 0.321$.

incorporated into Fig. 9 for comparison. It is noted that the definition of the Richardson numbers is Wang *et al.*[16] To have a consistent comparison, we re-expressed their data in terms of the Richardson number definition used in this study, i.e., $Ri = g'D/U_0^2$. The current results are in good agreement with the results of Gao and Yu[18] within the low Richardson number region ($-0.06 \le Ri \le 0.06$), and indicates a similar increasing trend of formation number against Ri for the moderate Richardson number range despite a lower slope. As shown in Fig. 9, when buoyancy effects are weak, $|Ri| < 0.1$, the formation number increases very rapidly against the Richardson number, whereas for $0.1 < Ri \le 0.321$ and $-0.1 > Ri \ge -0.321$, the rates of increase is slower. The results of Marugan-Cruz *et al.*[17] overestimate the effect of Richardson number on the variation of the formation number, in part due to the fact that they used the method of Ghairb *et al.*[4] for homogeneous starting jets to identify the buoyant formation number.

V. CONCLUDING REMARKS

In this paper, the process of vortex ring formation in starting buoyant jets with moderate Richardson numbers within the range of $0.06 < |Ri| \le 0.321$ is investigated numerically. A revised circulation model including the effects of buoyancy and over-pressure is derived by integrating the vorticity transport equation. Based on the results of the numerical simulation, it is found that the evolution of the leading vortex ring and trailing vortices is strongly affected by the buoyancy effect. As the positive Richardson number increases, the instabilities of the trailing jet occur earlier due to the entrainment and larger positive buoyancy acceleration. For the cases at moderate negative Richardson numbers, a "double plume" structure, i.e., the annular reverse flow with a negative vorticity layer around the inner sinking jet, can be observed. By using the similarity variables $|Ri|x_f/D$ and $|Ri|^{2/5}x_f/D$, the variation of dimensionless jet front penetration x_f/D with the formation time collapses on a single line for the positively and negatively buoyant jets, respectively. Based on the fitting equations of x_f/D, the revised buoyant circulation model (model 3) is well consistent with the numerical results for all positively buoyant jets. This demonstrates that the total circulation can be treated as a linear combination of the flux circulation due to the jet exit axial velocity and buoyant circulation due to the baroclinic production.

By adopting the revised circulation method, the buoyant formation number is found to become larger as the positive Richardson number increases, indicating that the pinch-off process of the leading vortex ring occurs later. As the negative buoyancy effect intensifies, the size and strength of the leading vortex gradually diminish, and the buoyant formation number keeps decreasing but at a lower rate than the variation of the formation number in the small Richardson number range.

ACKNOWLEDGMENTS

The authors acknowledge the support of the HKPolyU, Grant No. 1.4W.37.99QP, and the National Natural Science Foundation of China under Grant No. 11502153.

DATA AVAILABILITY

The data that support the findings of this study are available from the corresponding author upon reasonable request.

REFERENCES

[1]H. Suwa, Y. J. Suzuki, and A. Yokoo, "Estimation of exit velocity of volcanic plume from analysis of vortex structures," Earth Planet. Sci. Lett. **385**, 154–161 (2014).
[2]I. K. Bartol, P. S. Krueger, R. A. Jastrebsky, S. Williams, and J. T. Thompson, "Volumetric flow imaging reveals the importance of vortex ring formation in squid swimming tail-first and arms-first," J. Exp. Biol. **219**, 392–403 (2016).
[3]X. Bi and Q. Zhu, "Pulsed-jet propulsion via shape deformation of an axisymmetric swimmer," Phys. Fluids **32**, 081902 (2020).
[4]M. Gharib, E. Rambod, and K. Shariff, "A universal time scale for vortex ring formation," J. Fluid Mech. **360**, 121–140 (1998).
[5]J. O. Dabiri, "Optimal vortex formation as a unifying principle in biological propulsion," Annu. Rev. Fluid Mech. **41**, 17–33 (2009).
[6]N. Didden, "On the formation of vortex rings: Rolling-up and production of circulation," Z. Angew. Math. Phys. **30**, 101–116 (1979).
[7]D. I. Pullin, "Vortex ring formation at tube and orifice openings," Phys. Fluids **22**, 401–403 (1979).
[8]K. Shariff and A. Leonard, "Vortex rings," Annu. Rev. Fluid Mech. **24**, 235–279 (1992).
[9]A. Weigand and M. Gharib, "On the evolution of laminar vortex rings," Exp. Fluids **22**, 447–457 (1997).
[10]M. Rosenfeld, E. Rambod, and M. Gharib, "Circulation and formation number of laminar vortex rings," J. Fluid Mech. **376**, 297–318 (1998).
[11]P. S. Krueger, "An over-pressure correction to the slug model for vortex ring circulation," J. Fluid Mech. **545**, 427–443 (2005).
[12]P. S. Krueger, "Circulation and trajectories of vortex rings formed from tube and orifice openings," Physica D **237**, 2218–2222 (2008).
[13]M. Shusser, M. Gharib, M. Rosenfeld, and K. Mohseni, "On the effect of pipe boundary layer growth on the formation of a laminar vortex ring generated by a piston/cylinder arrangement," Theor. Comput. Fluid Dyn. **15**, 303–316 (2002).
[14]J. O. Dabiri and M. Gharib, "A revised slug model boundary layer correction for starting jet vorticity flux," Theor. Comput. Fluid Dyn. **17**, 293–295 (2004).
[15]R.-Q. Wang, A. W.-K. Law, E. E. Adams, and O. B. Fringer, "Buoyant formation number of a starting buoyant jet," Phys. Fluids **21**(12), 125104 (2009).
[16]R.-Q. Wang, A. W.-K. Law, and E. E. Adams, "Pinch-off and formation number of negatively buoyant jets," Phys. Fluids **23**, 052101 (2011).
[17]C. Marugán-Cruz, J. Rodríguez-Rodríguez, and C. Martínez-Bazán, "Formation regimes of vortex rings in negatively buoyant starting jets," J. Fluid Mech. **716**, 470–486 (2013).
[18]L. Gao and S. C. M. Yu, "Vortex ring formation in starting forced plumes with negative and positive buoyancy," Phys. Fluids **28**(11), 113601 (2016).
[19]L. Gao, H.-F. Guo, and S. C. M. Yu, "A general definition of formation time for starting jets and forced plumes at low Richardson number," J. Fluid Mech. **886**, A6 (2020).
[20]K. Mohseni and M. Gharib, "A model for universal time scale of vortex ring formation," Phys. Fluids **10**(10), 2436–2438 (1998).
[21]M. Krieg and K. Mohseni, "Modelling circulation, impulse and kinetic energy of starting jets with non-zero radial velocity," J. Fluid Mech. **719**, 488–526 (2013).
[22]I. Iglesias, M. Vera, A. L. Sánchez, and A. Liñán, "Simulations of starting gas jets at low Mach numbers," Phys. Fluids **17**, 038105 (2005).
[23]R.-Q. Wang, A. W.-K. Law, E. E. Adams, and O. B. Fringer, "Large-eddy simulation of starting buoyant jets," Environ. Fluid Mech. **11**, 591–609 (2011).
[24]C. Marugán-Cruz, J. Rodríguez-Rodríguez, and C. Martínez-Bazán, "Negatively buoyant starting jets," Phys. Fluids **21**(11), 117101 (2009).

[25]X. Zhou, Y. Xu, and W. Zhang, "Formation regimes of vortex rings in thermals," J. Fluid Mech. **885**, A44 (2020).
[26]Z.-Y. Li, Y. Xu, L.-H. Feng, and J.-J. Wang, "Synthetic jet vortex rings impinging onto a porous wall: Reynolds number effect," Int. J. Heat Mass Transfer **137**, 951–967 (2019).
[27]T. J. Mcdougall, "Negatively buoyant vertical jets," Tellus **33**(3), 313–320 (1981).
[28]N. Bhamidipati and A. W. Woods, "On the dynamics of starting plumes," J. Fluid Mech. **833**, R2 (2017).
[29]Y. J. P. Lin and Z. Y. Xu, "Buoyancy-driven flows by a heat source at different levels," Int. J. Heat Mass Transfer **58**, 312–321 (2013).
[30]R. Kumar and A. Dewan, "URANS computations with buoyancy corrected turbulence models for turbulent thermal plume," Int. J. Heat Mass Transfer **72**, 680–689 (2014).